Prepared for submission to JINST

Construction and test of a Small-Pads Resistive Micromegas prototype.

M.G. Alviggi,[a,b] **M. Biglietti,**[d] **V. Canale,**[a,b] **M. Della Pietra,**[a,b] **C. Di Donato,**[c,b,] **E. Farina,**[i] **S. Franchino,**[f] **P. Iengo,**[g] **M. Iodice,**[d] **F. Petrucci,**[e,d] **E. Rossi,**[e,d] **G. Sekhniaidze,**[b] **O. Sidiropoulou,**[g,h,] **V. Vecchio**[e,d]

[a] *Università di Napoli "Federico II",*
Corso Umberto I 40, 80138 Naples, Italy
[b] *INFN Napoli,*
Strada Comunale Cintia, 80126 Naples, Italy
[c] *Università di Napoli "Parthenope",*
Via Ammiraglio Ferdinando Acton 38, 80133 Naples, Italy
[d] *INFN Roma Tre,*
Via della Vasca Navale 84, 00146 Rome, Italy
[e] *Università di Roma Tre,*
Via della Vasca Navale 84, 00146 Rome, Italy
[f] *Heidelberg University,*
Grabengasse 1, 69117 Heidelberg Germany
[g] *European Center for Nuclear Research, CERN,*
Route de Meyrin 385, 1217 Meyrin, Switzerland
[h] *Bayerische Julius Max. Universität Wuerzburg, Sanderring 2, 97070 Würzburg, Germany*
[i] *Università di Pavia and INFN Pavia,*
Pavia,Italy

Abstract: Resistive micromegas is now a mature technology for High Energy Physics experiments. ATLAS experiment at CERN will upgrade the Muon Spectrometer (2019/2020) with 128 multilayers large size (O (2 m^2)) micromegas chambers. These detectors will operate at moderate hit rate up to about 15 kHz/cm^2 during the phase of High-Luminosity-LHC. Nevertheless, future upgrades and detectors at future accelerators will require operation at rates up to three orders of magnitude higher. In this paper we present the design, construction and test of micromegas with a small-pads resistive readout (few mm^2 in size) aiming at precision tracking in high rate environment without efficiency loss up to a few MHz/cm^2. The detector layout and the construction technique will be reviewed, along with a full characterization of its performance, carried out by means of radioactive sources, X-Rays and test beam.

Contents

1 Introduction

Developed in the '90s [1], MicroMegas' operation is based on its double gas gap structure, drift and amplification gaps, where respectively primary ionization and then avalanche multiplication take place. The drift region is generally few mm wide and is separated from the amplification region by a planar mesh electrode, kept at order of hundred microns with respect to the anode plane through a pillars matrix. First resistive [2] MicroMegas detectors were developed with a strip readout plane in view of the ATLAS NSW muon spectrometer upgrade [3], where high tracking efficiency was needed in a high background environment. The term 'resistive' refers to the presence of a resistive plane of strips on the top of the readout plane, with a kapton foil as insulator in between. This solution reduces possible discharges, quenched by the resistive layer, without spreading too much the avalanche footprint and produces a high efficiency detector (>98%) at rates up to 15 kHz/cm^2. To increase even more the measurable rate, up to tens of MHz/cm^2, we changed the resistive and readout planes from strips to small pads (O (mm^2)), lowering the detector occupancy. The proposed solution is inspired by a similar development considered for the COMPASS experiment [4] and based on a solution proposed by R. De Oliveira et al. in 2010 [5].

2 Small-Pads Resistive Micromegas construction details

The schematic concept of the first small-pad Micromegas (pad-MM) prototype detector built at CERN in 2015 [6] is shown if figure 1. The readout plane is segmented in pads 0.8×2.8 mm^2 wide with a pitch of 1×3 mm^2, covering a surface of 4.8×4.8 mm^2, forming a matrix with 48 pads

along the precise coordinate (that will be referred as x direction in the text) and 16 pads along the orthogonal direction (that will be named y direction), for a total number of 768 readout channels.

The resistive protection is obtained with a double layer of embedded resistors separated by a 12.5 μm thick Kapton foil. The resistors have the same size as the readout pads. The connection between the two layers of resistors and the readout pads is done with micro-vias in the Kapton, filled with silver-epoxy paste deposited by screen-printing. The vias on the two layer are staggered such that the electron current evacuated through the readout pads always sees at least one full embedded resistor. For a large fraction of the pads the resistance has been measured, obtaining values varying in a range 3–7 MΩ. The detector is completed with a bulk-Micromegas process [7], defining the 128 μm amplification gap with a metallic micro-mesh supported by Pyralux insulating pillars, and with a drift cathode defining the 5 mm wide conversion gap.

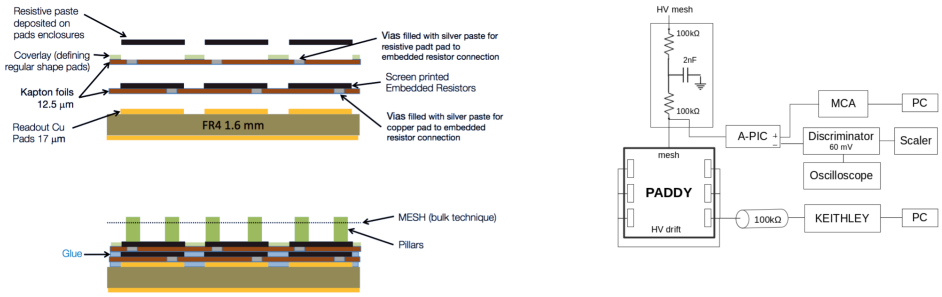

Figure 1. *left: schematic view of the detector. right: figure to be changed, substitute Keithley with picoammeter ...*

A different approach for the resistive layer has been tried in the construction of another prototype with the same readout segmentation. It was based on full screen printing of all layers (including the embedded resistor and the insulation layer) on top of the copper based anode board. This technique has several advantages. It is simple, cost effective and easy to scale to large size. Unfortunately, after the first tests, the detector has suffered from high voltage instabilities, and several attempts of reparation were not successful. The problem was possibly caused by the bad quality of the screen-printed insulation layer, between the anode and the top resistive pads, possibly developing pin-holes and causing discharges.

3 Detector characterization

The pad-MM prototype has been extensively tested in the GDD (Gas Detector Development) laboratory of the RD51 [8] collaboration at CERN, using different radiation sources and measuring its performances in different conditions. All the measurements have been carried out using Ar/CO_2 (93-7) gas mixture, focusing only on the intrinsic detector performance with a fixed gas amplification. Gain and electron transparency have been measured exposing the detector to ^{55}Fe sources with a different activity and to X-rays generated from a Cu target. The uniformity of the detector response has been also measured irradiating only a small part of the detector surface. Moreover, some tests

have been performed in different period showing a good stability of the detector performances across time.

3.1 Gain and Transparency measurements with ^{55}Fe

In order to measure detector gain and transparency, the pad-MM prototype has been exposed to an ^{55}Fe source. The experimental setup is described in fig. 1. The detector current is measured from all readout pads, connected to ground, through an high resolution picoammeter. The detector current is measured continuously (every each 400 ms) and stored in to a PC; fluctuations are mediated within a fixed time window (*WHO DOES REMEMBER THE CORRECT VALUE?*). Signal collected on the mesh goes first to a charge amplification stage and then to both a scaler and to a MultiChannel Analyzer (MCA). The charge preamplifier has been used with two different integration times of 30 ns or 300 ns.

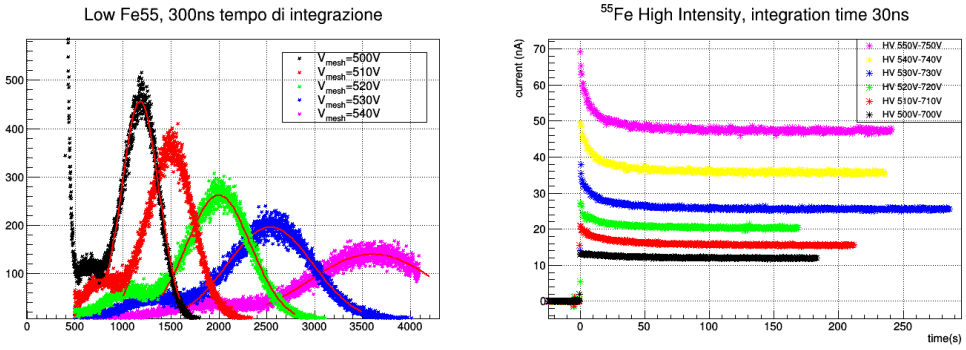

Figure 2. *left: energy spectra for FE55. right: detector current as a function of time for different amplification voltages*

Figure 2 left shows the energy spectra measured through the MCA for different detector amplification voltages, applied to the mesh, in the range between 500 and 540 V. The drift voltage was set to 200 V and the integration time of the charge preamplifier was set to 300 ns. We measured an energy resolution of about 35%. Figure 2 right shows the evolution of the current as function of the time measured with an integration time of 30 ns: a gain reduction of about 20% is clearly visible: this effect has been interpreted as a charging-up effect of the dielectric that surrounds the resistive pads.

Detector gain, defined as the ratio between the collected charge and the number primary electrons produced by the ionizing radiation, has been measured in different periods using ^{55}Fe sources with Low (corresponding to 1.3 kHz) and High (128 kHz) activities as a function of the amplification voltage: results are shown in figure 3 left. Two different methods have been used to measure the collected charge: or measuring the highest peak position from the MCA spectrum measuring the detector current and rate. The gain curves corresponding to the Low activity ^{55}Fe source are compatible with each other within measurement uncertainties even if the gain has been measured with different methods in different periods. The curve measured using the High activity ^{55}Fe source to irradiate the detector shows a gain reduction of about 20%. This measurement is in good agreement with the current reduction shown in figure 2 right and confirm the hypothesis of a

gain reduction due to a charging-up of the dielectric present on the readout surface, causing a local reduction of the amplification field.

Figure 3 right reports the relative electron transparency, measured as relative value of the ^{55}Fe spectra peak position, as function of amplification and drift electric field ratio: as expected the transparency reaches a plateau value above 95% for field ratio >100.

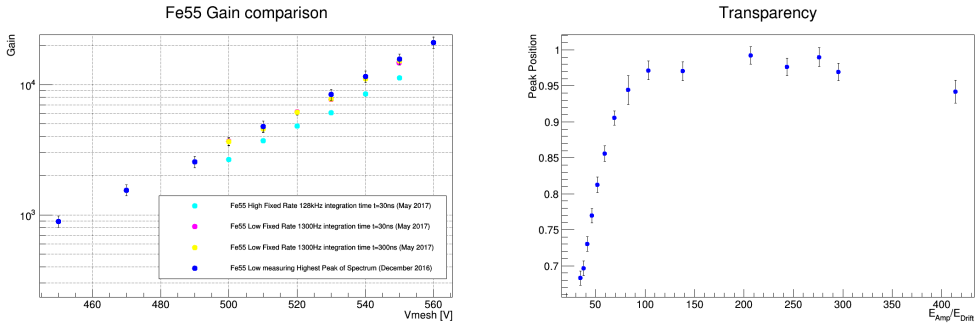

Figure 3. *left: Gain as a function of Amplification voltage for different Fe55 sources and different periods. right: Electron transparency as a function of amplification and drift electric field ratio.*

3.2 Irradiation tests with X-Rays

In order to measure the gain with an higher rate of incident particle the detector has been exposed to 8 keV peak energy X-rays from a Cu target tuning the intensity of the X-ray gun by varying the excitation current. Photons have been focused by using a 1 or 3 mm diameter collimator, or by shielding the detector active area with an absorber hosting a 10 mm diameter hole. In this way local rates of about 180 MHz/cm^2 have been reached. The experimental setup used during this measurement is the same described in 3.1 and shown in figure 1.

Figure 4 left shows the gain measured with an 10 mm hole for five different values of the amplification voltage is shown as a function of the photons rate. A gain reduction of about $\sim$ 20 % has been measured at 10 MHz/cm^2 photon rate for each amplification voltage value. To reach higher values of local photon rate a set of measurements have been done with a 3 mm collimator. Figure 4 right shows the gain measured using the 3 mm collimator for an amplification voltage of 530 V as a function of the photons rate in comparison with the measurements at the same amplification voltage with the 10 mm hole reported in figure 4 left. A further gain reduction, with smaller derivative, is visible: however the amplification gain of the detector is above 4000 up to a rate of $\sim$ 180 MHz/cm^2.

The modulation of the gain across the small (1 mm) and large (3 mm) dimension of the pads has been measured by moving, with a step of 0.1 mm, the relative position between the detector and the 1 mm collimator of the X-ray gun along the x and y axis, respectively. Figure 5 shows the results for the x and y scans, respectively. A maximum variation of the gain of about few percent, within a single pad, is measured. This modulation in gain reduction is compatible with the charging-up of the insulator hypothesis.

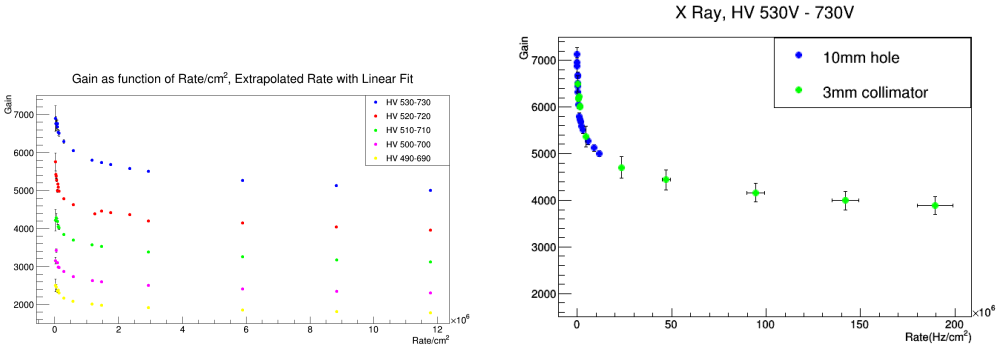

Figure 4. *left: Detector gain as a function of ionizing radiation rate for different amplification voltages. right: .*

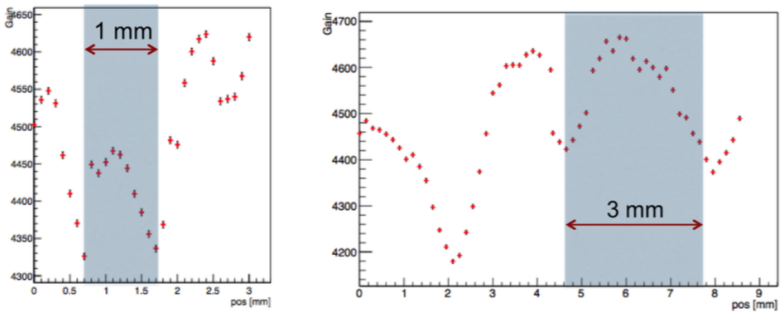

Figure 5. *Gain vs position. TO BE IMPROVED.*

4 Test Beam results

4.1 Experimental setup

The small-pad Micromegas prototype was exposed to high energy muons and pions beams at the CERN H4 beam line in October 2016 during the RD51 beam period.

The experimental setup consisted in the small-pad Micromegas and in two standard 10x10 cm^2 resistive-strips bulk Micromegas (Tmm chambers) with a double coordinate readout used as reference tracking chambers. The three detectors were placed on an aluminum support structure with the Tmm chambers at a distance of about 50 mm from the small-pad Micromegas, one upstream and one downstream. Two 100x100 mm^2 scintillators, placed before and after Tmm chambers, were used as a beam trigger. The active area of the trigger scintillators and of the Tmm chambers was larger than the 48x48 mm^2 of the small-pad Micromegas detectors. Only 2/3 of the strips of the Tmm chambers where read-out in both coordinates resulting in an area of about 60x60 mm^2. The detector positions were adjusted to have the available trigger and tracking area centred to cover the small-pad Micromegas surface.

The system was readout using a standard RD51 SRS system with one FEC connected to 14 APV25 readout boards via usb cables. 6 APV25 boards were used to readout the small-pad Micromegas prototype while 2 boards were needed for each view of each Tmm chamber.

The gas mixture (Ar/CO_2 93-7) was distributed in series to the detectors; the gas flux was such to have about xx gas volumes change per hour.

A reference system is defined with the z axis directed as the incoming beam particles, the y axis pointing to the ground and the x axis parallel to the ground. We call the x and y coordinates of the Tmm chambers and of the small-pad Micromegas accordingly to this definition. The precision coordinate (with 1 mm pitch) of the small-pad Micromegas was the x-coordinate while the second coordinate (with 3 mm pitch) was the y-coordinate.

Data were collected with the Tmm reference chambers at a fixed operating point (V_{amp}=xxx V, V_{drift}=xxx V) while changing the applied voltages of the small-pad Micromegas. The amplification voltage was varied from 440 V to 540 V while the drift voltage from xxx V to yyy V.

Both a high energy muon beam and a high intensity pion beam were exploited. With the pion beam, data were collected at different beam intensity. The beam intensity is expressed in the following by the trigger rate measured with the 100x100 mm^2 scintillators and varied from 35 to 400 kHz.

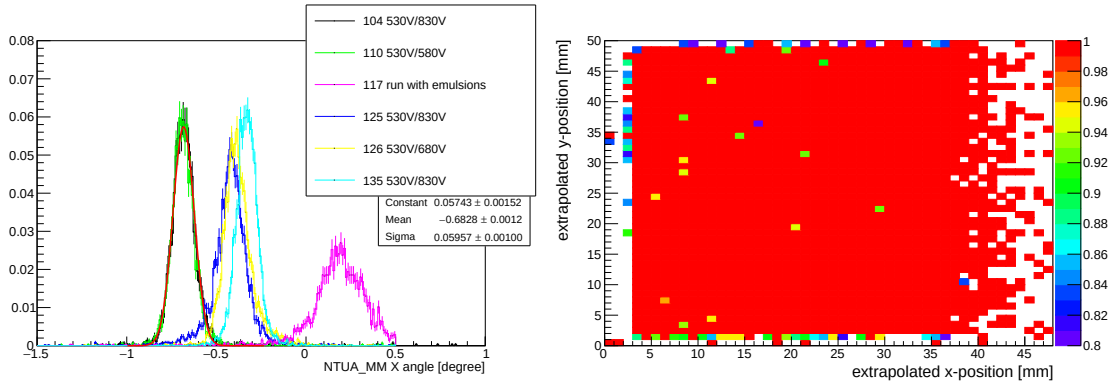

Figure 6. (left) ; (right) . - *(figure to be changed, at least labels to be improved, remove histo title, ...)*

4.2 Tracking system and events selection

Do we really want to add details about the "tracking performance"? The system is quite easy, maybe a couple of sentences are enough...

An event (i.e. a trigger from the two scintillators) was considered if only and only one cluster was reconstructed in both views of each one of the Tmm tracking chambers. This is to prevent any ambiguity in the track definition considering we have to rely on 2 measurements planes per each view. The fraction of good events ranges from 40% to 60% of the total, depending on the run and beam conditions. It has to be noted, that ~35% of the recorded events are discarded because the trigger area is larger than the instrumented area of the Tmm chambers.

From the clusters in both views of the Tmm chambers a reference track is fit and interpolated to the position of the small-pad Micromegas to measure resolution and efficiency. As an example, the reconstructed track angle in different runs in the x-coordinate is shown in Figure 6(left). The extrapolated position on the x-y plane of the pad-MM detector is shown in Figure 6(right).

Detectors positions and relative rotations were corrected offline with an iterative procedure looking at the distribution of the track residuals as a function of the x and y coordinates.

Considering a resolution of 100μm for a single cluster in the Tmm chambers, and interpolation error of ~50μm is obtained in the pad-MM detector position.

4.3 Detector performances

4.3.1 Cluster multiplicity, size and charge

To study the detector performance, pads charge and multiplicities distributions were addressed at first. The distribution of the pads charge is shown as an example in figure 7-left for two different runs with an amplification voltage of 440 V and 540 V respectively. A peak below 50 ADC is clearly visible and mostly due to noise hits. In the insert, a full range view of the distribution is shown. For the run at higher amplification voltage, the pads charge are higher and a saturation peak (due to the APV25 integration) is visible around 1800 ADC. To suppress the noise, a cut on the pads charge was imposed. It was set, separately for each channel, at 3 times the rms of the distribution of the ADC pedestal (runs with a random trigger were taken to measure the position and the rms width of the ADC pedestal for each channel). The distribution of the applied threshold for each channel is shown in figure 7-right.

Clusters within the small-pad Micromegas are reconstructed combining adjacent fired good pads. The cluster position is given by the weighted average of the pads positions (charge centroid).

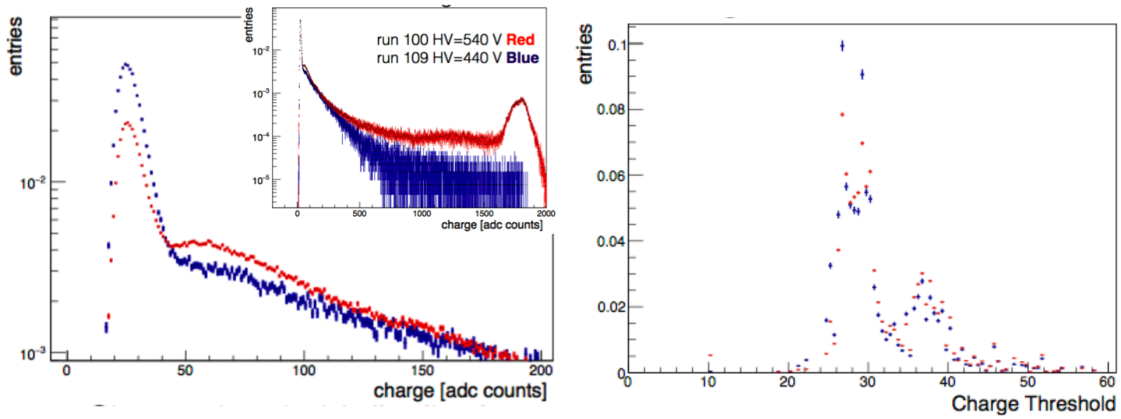

Figure 7. (left) pads charge distribution in two different runs with HV_{Amp}= 440V and HV_{Amp}= 540V, the distribution in the full range is shown in the insert; (right) Distribution of the charge threshold ($3\times\sigma_{ped}$) for each pad. - *(figure to be changed, at least labels to be improved, remove histo title, ...)*

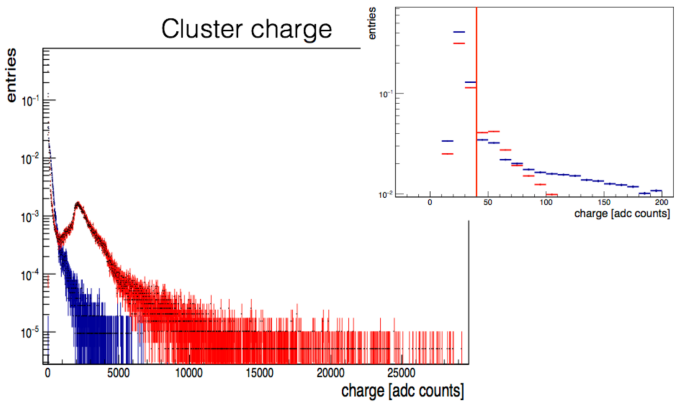

Figure 8. Cluster charge distribution in two different runs with HV_{Amp}= 440V and HV_{Amp}= 540V. A zoom is shown in the insert where the cut value of 40 ADC is also reported.- *(figure to be changed, at least labels to be improved, remove histo title, ...)*

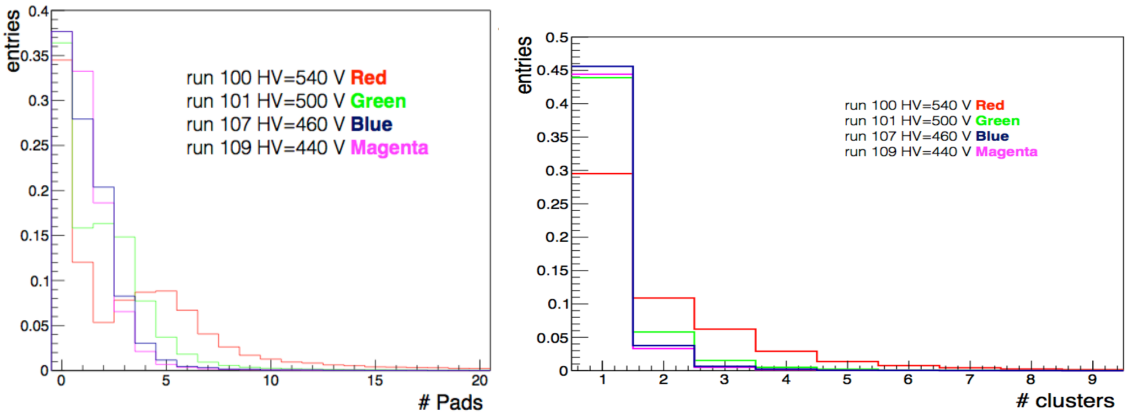

Figure 9. (left) Distribution of the number of pads per event for different values of the applied amplification voltage; (right) Distribution of the number of reconstructed clusters per event for different values of the applied amplification voltage.- *(figure to be changed, at least labels to be improved, remove histo title, ...)*

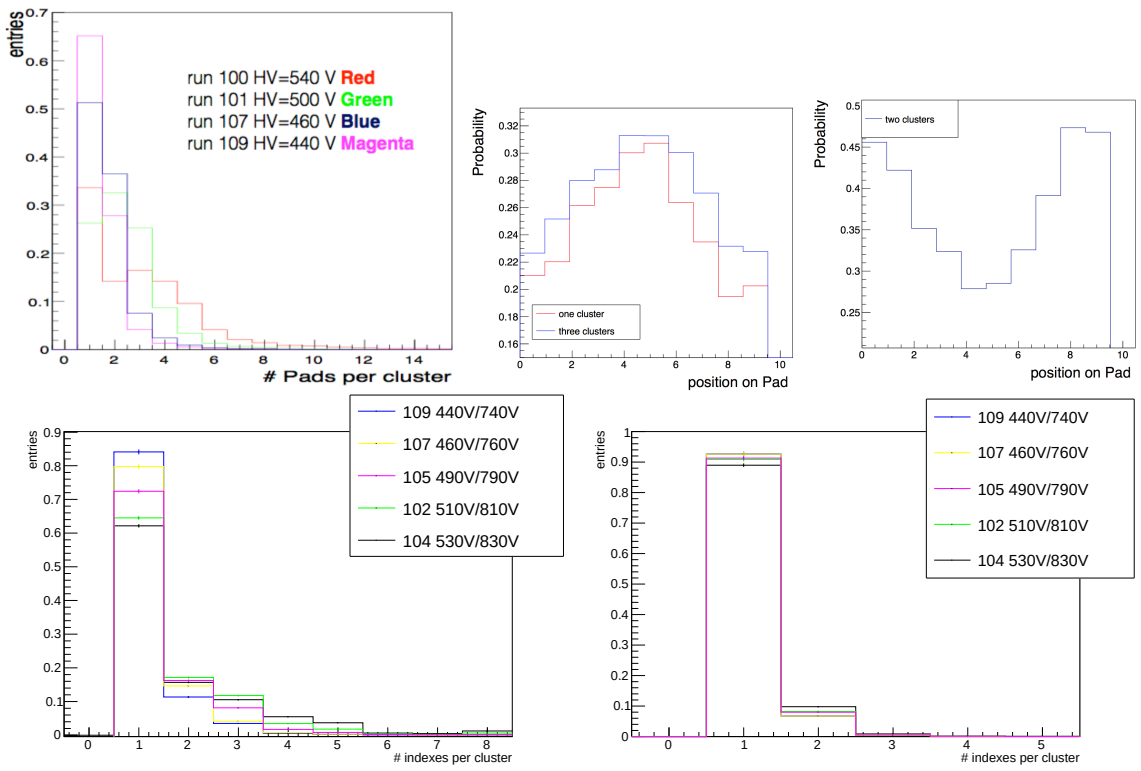

Figure 10. (upper-left) Distribution of the number of pads per cluster for different values of the applied amplification voltage; (upper-right) probability of firing an even or odd number of pads per cluster as a function of the position of the clusters centroid with respect to the pad; (lower-left) Distribution of the number of pads per cluster along the precision coordinate for different values of the applied amplification voltage; (lower-right) Distribution of the number of pads per cluster along the second coordinate for different values of the applied amplification voltage. - *(figure to be changed, at least labels to be improved, remove histo title, ...)*

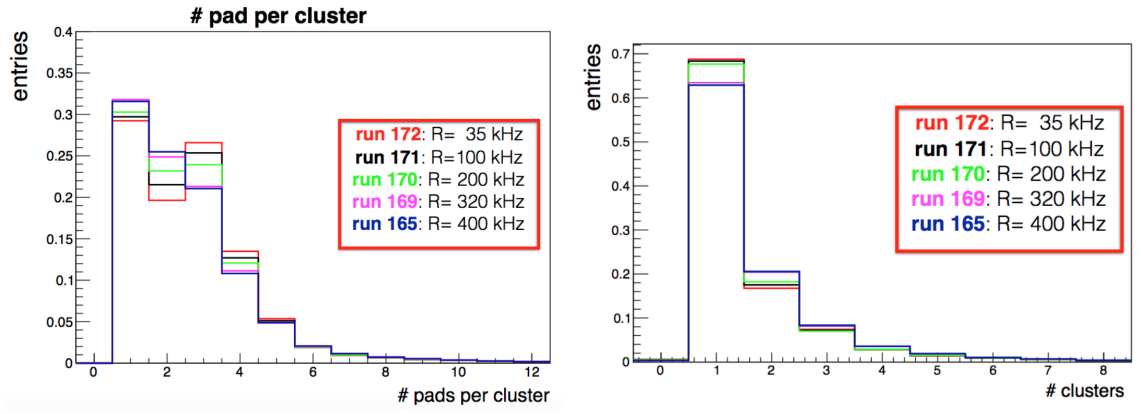

Figure 11. (Distribution of the number of pads per clusters (left) and of the number of clusters per event (right) for different values of the measured trigger rate in runs with pions beam.- *(figure to be changed, at least labels to be improved, remove histo title, ...)*

4.3.2 Spatial resolution

The position resolution is defined as the difference between the cluster position measured from the prototype and that interpolated by tracking chambers. In figure 6 the distribution of the residuals, in the precision coordinate, as measured with the high energy muon beam is reported. A spatial resolution of 190 ?m (from 1 mm pad pitch) was obtained.

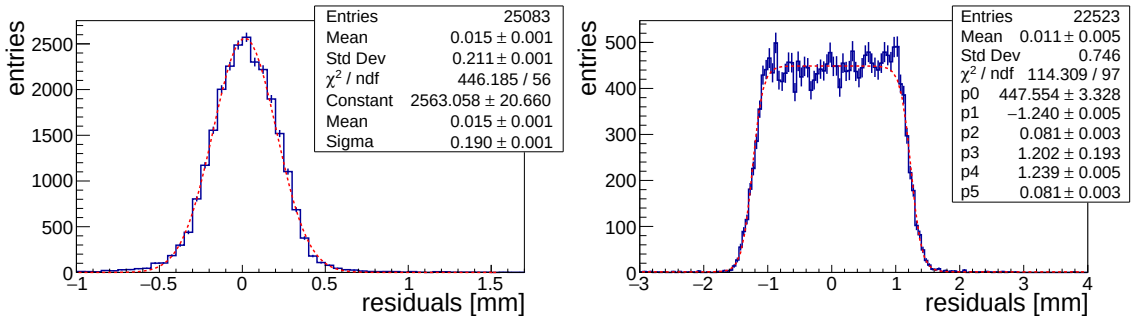

Figure 12. Residuals distribution in the precision 1 mm pitch coordinate (left) and in the second 3 mm pitch coordinate (right) as measured with an high energy muon beam for an amplification voltage of 530 V. - *(figure to be changed, at least labels to be improved, remove histo title, ...)* .

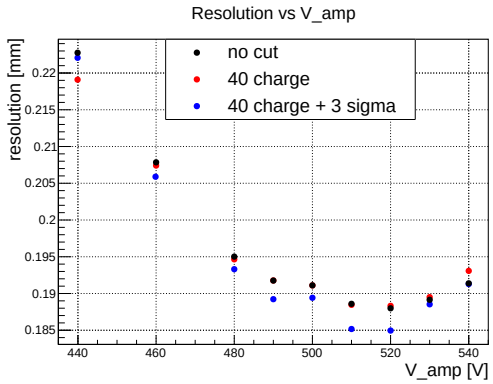

Figure 13. Spatial resolution in the precision coordinate as a function of the amplification voltage as measured with an high energy muon beam for different analysis cuts considering all the clusters (left) or only clusters with at least two pads (right). - *(figure to be changed, at least labels to be improved, remove histo title, ...)* .

4.3.3 Detector efficiency

The efficiency is measured checking, for each reference track, the presence of a cluster in the pad-MM prototype with different requirements: 1) a cluster anywhere in the detector (cluster efficiency); 2) a cluster within 1.5 mm from the extrapolated reference track (software efficiency); 3) a cluster within 5? (?1 mm) from the extrapolated reference track (5? efficiency). In figure 7 the cluster, software and 5? efficiencies as measured with the muon beam are shown as a function of the amplification voltage. The plateau is reached above 490 V with efficiencies of larger than 99

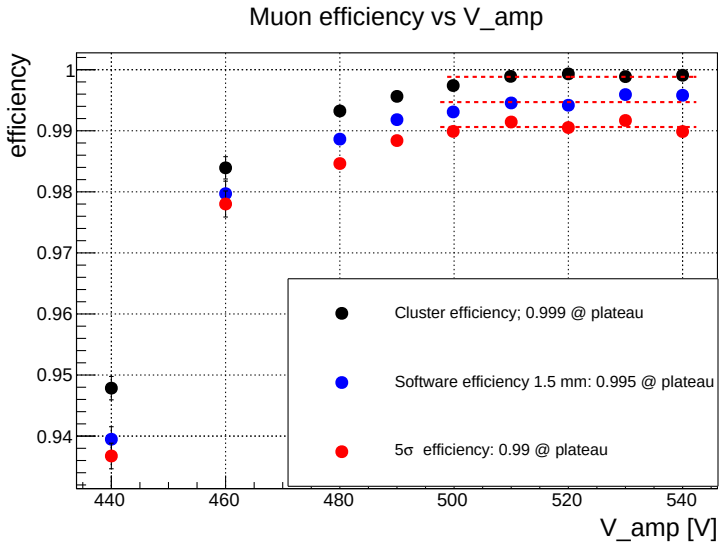

Figure 14. Detector efficiency as measured with a high energy muon beam.- *(figure to be changed, at least labels to be improved, remove histo title, ...)*

For pion beam analysis, do we want to use a kind of mean rate/(unit surface) to be defined somehow, instead of the trigger rate?

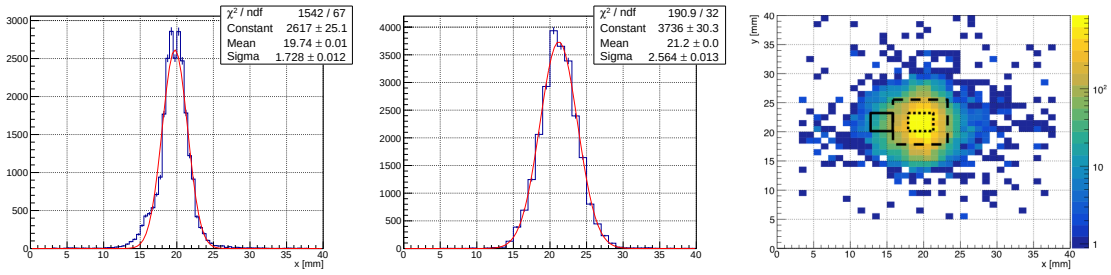

Figure 15. - *(figure to be changed, at least labels to be improved, remove histo title, ...)* .

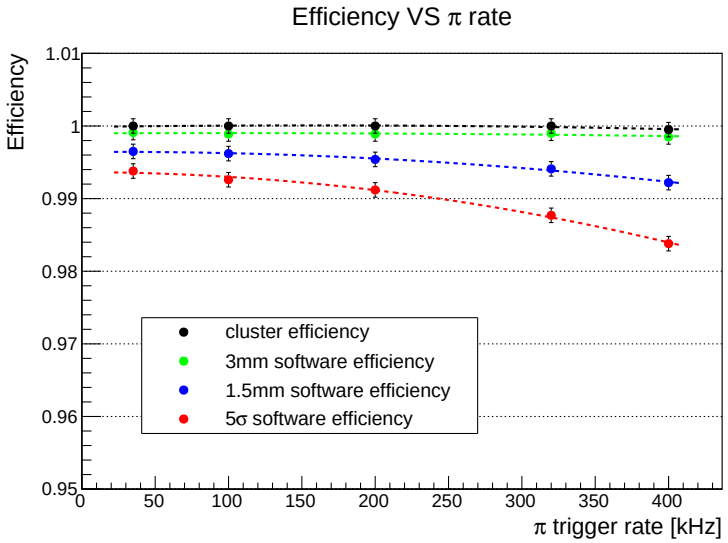

Figure 16. Detector efficiency as measured with a high intensity pion beam.- *(figure to be changed, at least labels to be improved, remove histo title, ...)*

References

[1] Y. Giomataris, P. Rebourgeard, J.P. Robert and G. Charpak, *MicroMegas: A high granularity position sensitive gaseous detector for high particle flux environments*, Nucl. Instrum. Meth. A 376 (1996) 29.

[2] T. Alexopoulos et al., *A spark-resistant bulk-MicroMegas chamber for high-rate applications*, Nucl. Instrum. Meth. A 640 (2011) 110.

[3] ATLAS collaboration, *New Small Wheel Technical Design Report*, CERN-LHCC-2013-006 (2013).

[4] F. Thibaud et al., *Performance of large pixelised MicroMEGAs detectors in the COMPASS environment*, 2014 JINST 9 C02005.

[5] R. de Oliveira, *Resistive protection in MicroMegas*, talk given at the RD51 Mini Week Workshop, CERN, Geneva Switzerland, 22–24 February 2010.

[6] M. Alviggi et al, *Small-pads resistive micromegas JINST* **12 C03077** (2017)

[7] I. Giomataris et al., *MicroMegass in a bulk*, Nucl. Instrum. Meth. A 560 (2006) 405 [physics/0501003].

[8] RD51 collaboration, *R&D Proposal Development of Micro-Pattern Gas Detector Technologies*, CERN-LHCC-2008-011 (2008).

[9] M.J. French et al., *Design and results from the APV25, a deep sub-micron CMOS front-end chip for the CMS tracker*, Nucl. Instrum. Meth. A 466 (2001) 359.

[10] S. Martoiu, H. Muller and J. Toledo, *Front-end electronics for the Scalable Readout System of RD51*, in the proceedings of Nuclear Science Symposium and Medical Imaging Conference (NSS/MIC), 23–29 October 2011.